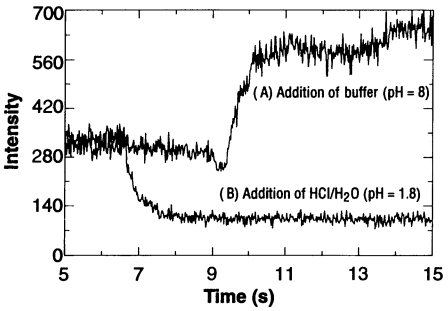

Fig. 5. Response time experiments at 25°C. The sensor (~80 μm) was first kept in air. During data acquisition, a pH 8 buffer was added to the container with the sensor (curve A). For curve B, a solution of HCl-H_2O (pH 1.8) was added to a container in which the sensor was immersed in a pH 6.86 buffer solution. Excitation at 488 nm was used for both experiments.

7.50 ± 0.05 for day 10 rat embryo) agree with those from "homogenized" samples (for example, pH 7.46 ± 0.06 for day 10 mouse embryos). Furthermore, the measurements carried out by our sensors are nondestructive single-cell operations. A complete embryo study will be reported (*16*).

Using four aqueous solutions in the physiological pH range (Table 1), we compared the accuracy of these optical fiber sensors to that of a macroscopic standard high-precision pH meter (Omega). The results from the sensor are similar to those obtained from the commercial pH meter and demonstrate the effectiveness of the internal calibration method in quantifying pH.

Because of the opposite effects of pH on absorptivity at different wavelengths (Fig. 3), we made use of the differences both in absorption and in fluorescence of the dye at different wavelengths to quantify the pH and increase the differential in intensity ratio per pH unit change. We obtained a significant enhancement factor (Table 2).

The miniaturization of the sensor also permits a very fast response time because the analytes have immediate access to the dye on the sensor tip. The submicrometer sensors have response times shorter than can presently be measured (20 ms). This is consistent with Fig. 5, which shows the 10 to 90% response times for one of our largest sensors (~80 μm) to be ≤500 ms.

The submicrometer pH sensor has a detection limit of ≤3000 hydrogen ions in the measurements of pH 8 buffer solutions inside a micrometer-size membrane hole (*13*). The submicrometer pH sensor also has good stability, even when a high laser power (30 mW, collected fluorescence intensity around 10^5 counts per second) is used. Over a time period of 40 min, only a 10% loss in intensity for sensors immersed inside a buffer solution was recorded. The photobleaching is practically imperceptible at the routine lower laser power operation.

REFERENCES AND NOTES

1. M. A. Arnold and M. E. Meyerhoff, *CRC Crit. Rev. Anal. Chem.* **20**, 145 (1988).
2. W. R. Seitz, *Anal. Chem.* **56**, 16 (1984); *CRC Crit. Rev. Anal. Chem.* **19**, 135 (1988).
3. O. S. Wolfbeis, *Fiber Optic Chemical Sensors and Biosensors* (CRC Press, Boca Raton, FL, 1991), vol. 1.
4. S. M. Barnard and D. R. Walt, *Nature* **353**, 338 (1991); C. Munkholm, D. R. Walt, F. M. Milanovich, S. M. Klainer, *Anal. Chem.* **58**, 1427 (1986).
5. R. Kopelman, *Science* **241**, 1620 (1988).
6. E. Betzig, J. K. Trautman, T. D. Harris, J. S. Weiner, R. L. Kostelak, *ibid.* **251**, 1468 (1991).
7. R. Kopelman *et al.*, *SPIE J.* **1637**, 33 (1992).
8. A. Lewis and K. Lieberman, *Anal. Chem.* **63**, 625 (1991).
9. L. M. Christian and W. R. Seitz, *Talanta* **35**, 119 (1988); Z. Zhang and W. R. Seitz, *Anal. Chim. Acta* **160**, 47 (1984).
10. S. Luo and D. R. Walt, *Anal. Chem.* **61**, 174 (1989).
11. K. Lieberman, S. Harush, A. Lewis, R. Kopelman, *Science* **247**, 59 (1990).
12. W. Tan, R. Kopelman, K. Lieberman, A. Lewis, in *Dynamics in Small Confining Systems*, J. M. Drake, J. Klafter, R. Kopelman, Eds. (Materials Research Society, Pittsburgh, PA, 1990), pp. 195–198.
13. W. Tan, Z.-Y. Shi, R. Kopelman, *Anal. Chem.*, in press.
14. C. Harris, *Teratology* **43**, 229 (1991).
15. H. Nau and W. J. Scott, *Arch. Toxicol.* (suppl. 11), 128 (1987).
16. W. Tan, B. A. Thorsrud, C. Harris, in preparation.

17. We thank B. Thorsrud and C. Harris for providing rat embryo samples and S. Parus for computer programming. We also thank M. Meyerhoff, M. Morris, M. Shortreed, and D. Walt for helpful discussions. Supported by Department of Energy grants DE-FG02-90ER 60984 and DE-FG02-90ER 61085.

5 June 1992; accepted 14 August 1992

Large Enhancement in Oxygen Mobility in the Superconductors $RBa_2Cu_3O_7$ with Increasing Rare-Earth Size

J. L. Tallon and B.-E. Mellander*

Ultrasonic composite oscillator measurements of the mechanical relaxation in $RBa_2Cu_3O_{7-\delta}$ arising from oxygen hopping in the basal chain layer show enhancements in oxygen mobility of 20, 50, and 100 times for R = gadolinium, neodymium, and lanthanum, respectively, above that for R = yttrium. The use of the larger rare earths offers a practical solution to the major problem of slow oxygen diffusion in single crystals and bulk, dense material for wires and melt-textured monolithic bodies.

Solid-state oxygen diffusion is of interest in a range of disciplines and technologies from diffusion in minerals for geothermometers and geobarometers (*1*), to fast oxygen ion conductors for fuel cells and oxygen sensors (*2*), to electronic ceramics (*3*), to cuprate superconductors with high superconducting transition temperatures, T_c (*4*). The 90 K superconductors $RBa_2Cu_3O_{7-\delta}$ (R = Y, La, Nd, . . .) are oxygen-deficient ($\delta > 0.7$) as synthesized and, as a consequence, insulating. An essential step in their manufacture is to load oxygen after synthesis by annealing or slow cooling in O_2 to 350°C to induce superconductivity. The transition temperature is maximized at about 90 K when oxygen deficiency is more or less eliminated and $0 \leq \delta \leq 0.1$. Oxygen diffusion into and through the lattice occurs in the basal chain layer between the ideally occupied O1 site and the ideally unoccupied O5 site. This incorporation of oxygen presents no difficulty in conventionally prepared materials in which, because of their high porosity (>15%) and microcracks, oxygen is able to diffuse rapidly into the material bulk. Moreover, because of the $T_c \approx 90$ K plateau (*4*), incomplete oxygen loading may result in a 90 K superconductor, although other properties, such as flux pinning, will not be optimized.

Dense, bulk material presents a rather different picture. Because the oxygen self-diffusion coefficient between 400° and 500°C is in the range 10^{-12} to 10^{-11} cm^2/s, the rate of oxygen loading in $YBa_2Cu_3O_{7-\delta}$ (1-2-3) may be prohibitively slow for samples that are more than 98% dense and several millimeters in dimension (*5*). In addition, the markedly anisotropic thermal strains (*4*) that occur on oxygen loading (positive in the *b* direction and negative in the *a* direction), as well as the effects of inhomogeneous oxygen loading, result in differential stresses that cause substantial microcracking. This change in microstructure, of course, has a harmful effect on critical current density and on mechanical properties.

It was earlier shown (*6*) that, by substituting A = Na, K, or Ca into 1-2-3 according to the formula $Y_{1-x}Ba_{2-y}A_{x+y}Cu_3O_{7-\delta}$ ($x + y$

New Zealand Institute for Industrial Research and Development, Post Office Box 31310, Lower Hutt, New Zealand.

*Permanent address: Department of Physics, Chalmers University of Technology, Gothenburg, Sweden.

≤ 0.1), it was possible to achieve giant enhancements of up to 100-fold in oxygen loading rates. There appeared to be no change in microstructure associated with these substitutions. Rather, ultrasonic mechanical damping studies showed the appearance of fast relaxation processes, which indicated enhancement in the bulk-diffusion rate. However, we do not consider these substituents to be practical for bulk, high-critical-current applications because the alkali ions greatly reduce the stability to atmospheric attack (6) and Ca significantly depresses T_c (7, 8).

The motivation behind the present work is that, by choosing R to be a larger lanthanide ion, the size of the 1-2-3 lattice cage is increased and the oxygen diffusion coefficient should inevitably be larger. In addition, provided one can suppress the tendency for the larger lanthanides to partially substitute on the Ba site, T_c progressively rises toward 100 K. We examined ultrasonic relaxation at 40 kHz in 1-2-3 with R = Y, Gd, Nd, and La and found enhancements in the oxygen relaxation rate (and hence in the oxygen self-diffusion coefficient) of 19, 48, and 97 times, respectively, for the larger rare earths relative to Y. The present, almost exclusive, use of Y-123 for wires and bulk applications has been locked into practice for historical reasons but would appear to be inappropriate from the perspective of oxygen diffusion.

We prepared Y-123 and Gd-123 with $Ba(NO_3)_2$, CuO, and Y_2O_3 or Gd_2O_3, respectively. The milled mixture was decomposed at 700°C for 1 hour, then ground, milled, and die-pressed into pellets and reacted twice for 14 hours at 910°C in air with intermediate grinding. The pellets were then ground, milled, and die-pressed into bars 3.5 by 3.5 by 60 mm. These were reacted in flowing oxygen for 14 hours and then slow-cooled to 400°C and held at that temperature overnight. The zero-resistance T_c for Y-123 and Gd-123 samples was 92 and 93 K, respectively. The Nd-123 sample was prepared in similar fashion at 900°C and then 920°C, except that each reaction was in a flowing gas mixture of 0.02% O_2 mixed with N_2. The reaction vessel was evacuated and backfilled with the gas mixture to ensure that the sample was not exposed to a higher O_2 partial pressure during the early stages of synthesis and sintering. This process is essential to suppress partial substitution of Nd for Ba, which is evidenced by the appearance of the impurity phase $BaCuO_2$ in x-ray diffraction patterns. The zero-resistance T_c for this sample was 95 K. The La-123 sample was prepared in the same fashion except that only N_2 gas was used. This sample, against the trend, had a lower T_c ~91 K, which arises, we believe, from the residual partial substitution of La for Ba. The resistive transition for this compound was significantly broadened as is typical of an underdoped high-T_c superconductor with a small degree of substitutional disorder (9). In contrast, the Y, Gd, and Nd compounds all had similarly narrow resistive transitions indicative of good stoichiometric compositions. These three compounds were 85 to 86% dense, and the La-123 sample was 92% dense. Lattice parameters for each of these compounds were determined by x-ray powder diffraction.

Ultrasonic composite oscillator measurements were carried out in the longitudinal mode as described previously (10). Briefly, the composite oscillator consists of a quartz drive crystal, quartz gauge crystal, and a fused quartz spacer rod with a length equal to 2.5 wavelengths terminated by the sample rod, all glued end to end. The joint between sample and fused quartz was made with Sauereisen ceramic cement cured for 1 week. The samples were cut to a resonant length for a frequency of 40 kHz at ~500°C. The composite oscillator was mounted in a vacuum system with the sample end projected into a furnace. A closed-loop amplifier was used to drive the composite oscillator in a constant gauge voltage mode, that is, at constant strain amplitude. We determined the Young's modulus and the mechanical damping or internal friction, Q^{-1}, of the sample, respectively, from the frequency and the ratio of the drive to gauge voltages using standard relations (10).

Data were collected at 700°C at heating and cooling rates of 67°C per hour in 100, 20, and 2% O_2 in N_2 at 1 bar. Results were essentially reproducible whether heating or cooling, indicating that there was little hysteresis attributable to oxygen unloading and reloading. The technique has been used extensively for $YBa_2Cu_3O_{7-\delta}$ (5, 6, 10). A Debye relaxation peak occurs at ~800 K, which results from the hopping of oxygen atoms between the O1 and O5 intrachain and interchain sites. Diffusion coefficients calculated from the measured relaxation times agree satisfactorily with ^{18}O tracer diffusion measurements (5, 11). Across a broad temperature range the relaxation time and self-diffusion coefficient have a simple Arrhenius dependence over six orders of magnitude with an activation energy of 1.04 eV.

Lattice parameters for each of the samples are listed in Table 1. The data show a progression to larger values as the ion size (also listed) increases. As reported for Y-123 (10), the Young's modulus for all samples exhibits a deep soft-mode cusp at the orthorhombic-tetragonal (O-T) transition due to orthorhombic fluctuations. The O-T transition temperatures (T_{O-T}) in an atmosphere of 20% O_2 in N_2 are listed in Table 1, and these progress to lower temperatures as the orthorhombicity decreases with increasing ion size. The T_{O-T} values are largely in agreement with data (12) from thermal gravimetry and resistivity measurements. However, the measured T_{O-T} for La-123 is significantly higher than the earlier data.

Table 1. Measured data for Y-123, Gd-123, Nd-123, and La-123: ion size, r_i (14); lattice parameters, a, b, and c; orthorhombic-tetragonal transition temperature T_{O-T}; temperature T_m at the maximum in the damping peak; and $D_m(R)/D(Y)$, ratio of the diffusion coefficient for each lanthanide ion at T_m to that for Y-123 at the same temperature.

Parameter	R			
	Y	Gd	Nd	La
r_i (Å)	1.019	1.053	1.109	1.160
a (Å)	3.822	3.842	3.862	3.893
b (Å)	3.887	3.899	3.918	3.938
c (Å)	11.680	11.699	11.771	11.818
T_{O-T} (°C)	645	610	564	560
T_m (°C)	543	408	374	350
$D_m(R)/D(Y)$	1	19	48	97

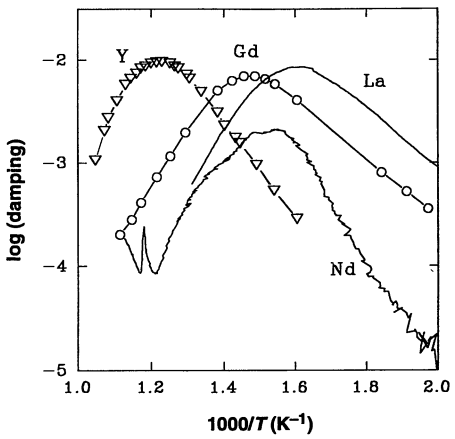

Fig. 1. Plot of the mechanical damping versus inverse temperature for R = Y, Gd, Nd, and La.

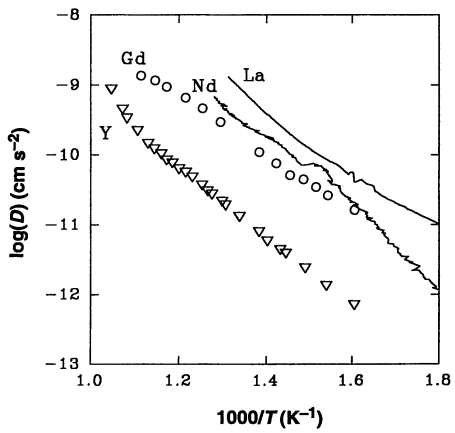

Fig. 2. Plot of the oxygen self-diffusion coefficient versus inverse temperature for R = Y, Gd, Nd, and La.

Figure 1 shows an Arrhenius plot of the temperature dependence of the mechanical damping of $RBa_2Cu_3O_{7-\delta}$ in equilibrium with an ambient atmosphere of 20% O_2 in N_2 for R = Y, Gd, Nd, and La. As anticipated, the relaxation peaks at a fixed frequency of 40 kHz were displaced to progressively lower temperatures (543°, 408°, 374°, and 350°C, respectively) as the rare-earth size was increased. Over this temperature range, the relaxation for $YBa_2Cu_3O_{7-\delta}$ is thermally activated with a single activation energy of motion $h_m \sim 1.04$ eV (*5*). At the location of the mechanical damping maxima, the enhancements in mobility over that for R = Y are, respectively, 19, 48, and 97 times for R = Gd, Nd, and La. These major enhancements occur in the temperature range that is relevant for loading oxygen. The temperatures T_m for maximum damping and the enhancements in diffusion coefficients are also listed in Table 1.

Oxygen self-diffusion coefficients, D, may be estimated by assuming that the damping, Q^{-1}, is governed by a single Debye relaxation, which is thermally activated. Thus

$$Q^{-1} = Q_0^{-1}\omega\tau/(1+\omega^2\tau^2) \quad (1)$$

where ω is the frequency and τ is the relaxation time, and

$$\tau = \tau_0 exp(h_m/kT) \quad (2)$$

where k is the Boltzmann constant. Oxygen diffusion occurs by two-dimensional hopping between the O1 and O5 sites, so that

$$D = f\ell^2/4\tau \quad (3)$$

where f is the correlation factor and $\ell \sim 2.76$ Å is the hop distance between the O1 and O5 sites. The temperature dependence of D or τ is large compared with that of f, so we assume for convenience $f \sim 1$. The values of D thus calculated (plotted in Fig. 2) show a clear progression to higher oxygen diffusion rates in lattices containing the larger rare-earth ions. At a fixed temperature of 400°C the enhancements in D over that for Y-123 are 19, 30, and 56 times for Gd-, Nd-, and La-123, respectively. The diffusion coefficient relevant to oxygen loading is the chemical diffusion coefficient, which is related to the self-diffusion coefficient, measured here, by a factor that describes the dependence of the oxygen stoichiometry, δ, on oxygen partial pressure. Kishio *et al.* (*12*) reported the temperature and oxygen partial pressure dependence of δ at equilibrium to be very similar for Y-123 and Nd-123. We therefore expect that the large enhancements in diffusion coefficient reported here will also be reflected in oxygen chemical diffusion coefficients.

Data from the tails of the relaxation peaks are not reliable because of the dominance there of background damping and because of the large excursion from tuned resonance, which we imposed in mid-temperature range by trimming the length of both the sample and the quartz spacer rod. The Nd-123 data appear to be particularly affected in this way. The data are also critically dependent on the quality of the ceramic joint between the sample and the spacer rods. We have extended measurements to much longer relaxation times (~24 hours) by examining the transient relaxation of structure at room temperature by in situ x-ray diffraction after quenching from elevated temperatures into liquid N_2. The same trend in enhanced mobility with the larger rare earths is preserved, but the enhancements are much smaller (approximately fourfold) (*13*).

REFERENCES AND NOTES

1. S. M. Fortier and B. J. Giletti, *Science* **245**, 1481 (1989).
2. C. G. Vayenas, S. Bebelis, S. Ladas, *Nature* **343**, 625 (1990).
3. B. C. H. Steele, *Electronic Ceramics* (Elsevier, New York, 1991).
4. J. D. Jorgensen *et al.*, *Phys. Rev. B* **41**, 1863 (1990).
5. J. L. Tallon and M. P. Staines, *J. Appl. Phys.* **68**, 3998 (1990).
6. J. L. Tallon *et al.*, *Physica C* **171**, 61 (1990).
7. A. Manthiram, S. J. Lee, J. B. Goodenough, *J. Solid State Chem.* **73**, 278 (1988).
8. R. G. Buckley *et al.*, *Physica C* **174**, 383 (1991).
9. J. L. Tallon *et al.*, *ibid.* **185–189**, 855 (1991).
10. J. L. Tallon, A. H. Schuitema, N. E. Tapp, *Appl. Phys. Lett.* **52**, 507 (1988).
11. S. J. Rothman, J. L. Routbort, U. Welp, J. E. Baker, *Phys. Rev. B* **44**, 2326 (1991).
12. K. Kishio *et al.*, *Mater. Res. Soc. Symp. Proc.* **156**, 91 (1989).
13. J. L. Tallon and B.-E. Mellander, in preparation.
14. R. D. Shannon, *Acta Crystallogr. Sect. A* **32**, 751 (1976).

15. We are grateful to the New Zealand Foundation for Science, Research, and Technology and to the Electricity Corporation of New Zealand for funding this research. We thank R. G. Buckley and W. H. Robinson for discussing aspects of this work.

29 May 1992; accepted 25 August 1992

Nanochannel Array Glass

R. J. Tonucci, B. L. Justus, A. J. Campillo, C. E. Ford

The fabrication and characterization of a glass containing a regular parallel array of submicrometer channels or capillaries are described. The capillaries are arranged in a two-dimensional hexagonal close packing configuration with channel diameters as small as 33 nanometers and packing densities as high as 3×10^{10} channels per square centimeter. The high-temperature stability of the nanochannel glass array is well suited as a host or template for the formation of quantum confined semiconductor structures or as a mask for massively parallel patterned lithographic applications.

Quantum confined systems imbedded in a protective or interactive matrix have generated considerable interest in both basic research and commercial applications because of their unique electronic and optical properties and their possible use as components in ultrasmall and ultradense electronic devices (*1*, *2*). One such approach to fabricating quantum confined structures has been to utilize a host or template structure. Very small chambers or voids within the host can be filled with material in which the walls of the void confine the volume of material being deposited. If the voids are sufficiently small (*3*), quantum confinement may occur in the material and its associated quantized effects observed by a variety of optical and electronic measurements. Examples utilizing this technique to create quantum confined systems with II-VI and III-V semiconductor materials have been demonstrated in a variety of host structures such as zeolites (*4*), plastics (*5*, *6*), sol-gels (*7*, *8*), and Vycor glass (*9*, *10*).

Nanochannel glass (NCG) hosts and masks with uniformly shaped voids in large arrays exhibit a high packing density of parallel voids or channels with channel diameters as small as a few tens of nanometers (*11*). There are greater than 10^6 channels in a typical array and excellent control is maintained over the geometric regularity in the placement of channel positions as well as the depth of channel formation.

The fabrication of this NCG material is inspired by a draw process not unlike the way optic fibers and microchannel plates are made (*12*, *13*). Recent attempts at drawing single glass fibers have succeeded in producing hollow (*14*) and metal-filled (*15*) cores as small as a few tenths of a micrometer. The smallest previously reported high-density glass fiber arrays made by a drawing process containing greater than 10^6 channels exhibited channel diameters of approximately 2 μm (*16*).

Nanochannel glass arrays are prepared by arranging dissimilar glasses, of which at

R. J. Tonucci, B. L. Justus, A. J. Campillo, Optical Sciences Division, Naval Research Laboratory, Washington, DC 20375.
C. E. Ford, Ni-Tec Division, Varo Inc., Garland, TX 75041.